Environmental Research Letters

LETTER • **OPEN ACCESS**

Estimating site-specific optimum air temperature and assessing its effect on the photosynthesis of grasslands in mid- to high-latitudes

To cite this article: Qing Chang *et al* 2020 *Environ. Res. Lett.* **15** 034064

Environmental Research Letters

LETTER

OPEN ACCESS

RECEIVED
1 September 2019

REVISED
15 January 2020

ACCEPTED FOR PUBLICATION
28 January 2020

PUBLISHED
6 March 2020

Estimating site-specific optimum air temperature and assessing its effect on the photosynthesis of grasslands in mid- to high-latitudes

Qing Chang[1], **Xiangming Xiao**[1], **Xiaocui Wu**[1], **Russell Doughty**[1], **Wenzhe Jiao**[2], **Rajen Bajgain**[1], **Yuanwei Qin**[1] and **Jie Wang**[1]

[1] Department of Microbiology and Plant Biology, Center for Spatial Analysis, University of Oklahoma, Norman, OK 73019, United States of America

[2] Department of Earth Sciences, Indiana University-Purdue University Indianapolis (IUPUI), Indianapolis, IN 46202, United States of America

E-mail: xiangming.xiao@ou.edu

Keywords: eddy flux tower sites, gross primary productivity, EVI, vegetation productivity model

Supplementary material for this article is available online

Abstract

The effect of air temperature on photosynthesis is important for the terrestrial carbon cycle. The optimum air temperature for photosynthesis is one of the major parameters in data-driven and process-based photosynthesis models that estimate the gross primary production (GPP) of vegetation under a changing climate. To date, most models use the biome-specific optimum air temperature (T_{opt-b}) parameter. To what degree will the site-specific optimum air temperature (T_{opt-s}) affect GPP simulation results remains unclear. In this study, we estimated T_{opt-s} by using GPP data from 11 grassland eddy flux tower sites (GPP_{EC}) and satellite vegetation indices (NDVI and EVI). We found that $T_{opt\text{-}s}$ parameter values estimated from EVI have good consistency with those from GPP_{EC} at individual sites. We also evaluated the effects of site-specific and biome-specific optimum air temperature parameters on grassland photosynthesis. The results showed that the use of T_{opt-s} in the Vegetation Photosynthesis Model improved to various degrees in both daily and annual GPP estimates in those grassland flux tower sites. Our results highlight the necessity and potential for the use of T_{opt-s} in terrestrial GPP models, especially in those situations with large temperature variation (heatwave and cold spill events).

1. Introduction

The relationship between air temperature and photosynthesis or gross primary production (GPP) of vegetation at the local, regional, and global scales has been studied over many decades (Williams *et al* 2014; Huang *et al* 2019). Global warming and climatic extremes (e.g. heatwaves and cold spills) have large impacts on vegetation production across space and time (Mu *et al* 2011; Jiao *et al* 2019a; Ryu *et al* 2019). Accurately quantifying the effects of air temperature on the GPP of vegetation at local, regional, and global scales is critical to improving the modeling of GPP and terrestrial carbon cycles.

In addition to process-based biogeochemical models (Sellers *et al* 1986; McGuire *et al* 1995; Zhang *et al* 2012), satellite-based data-driven biogeochemical models have proven to be a great tool for estimating GPP, as satellite-based sensors provide continuous observations across local, regional, and global scales, especially for regions with limited *in situ* observations. A number of satellite-based terrestrial carbon models have been developed and used to estimate GPP at various spatial scales (Potter *et al* 1993; Xiao *et al* 2004a; Zhao *et al* 2005; Turner *et al* 2006; Jiang and Ryu 2016; Ryu *et al* 2019). Most of these satellite-based GPP models are designed on the basis of the production efficiency concept, also known as light use efficiency (LUE) or the radiation use efficiency concept (table S1, available online at stacks.iop.org/ERL/15/034064/mmedia). These LUE models estimated daily GPP based on photosynthetically active radiation (PAR) absorbed by vegetation (APAR) and LUE (ε) ($GPP = APAR \times \varepsilon$). In these models, the LUE (ε)

parameter is often estimated as the product of the potential or maximum LUE (ε_0) and a few down-regulation scalars such as temperature, precipitation, soil moisture, vapor pressure deficit, and leaf age (Monteith 1972, 1977; Prince and Goward 1995).

Temperature constraint, represented by temperature scalar (T_s), has been used in most LUE models (table S1). The typical response of leaf-level photosynthesis to temperature can be described by a bell-shaped relationship (Berry and Bjorkman 1980; Cox 2001; Clark *et al* 2011; Landsberg *et al* 2011). Because of the limitation of electric transport and Rubisco activity, plants tend to have low photosynthesis at cool temperatures, and increase to a maximum rate at optimal temperatures in the 20 °C–30 °C range and then decrease again at very high temperatures (Fitter and Hay 2012). This optimum temperature (T_{opt}) response has been described across a wide range of plant species (Kirschbaum and Farquhar 1984; Battaglia *et al* 1996; Fitter and Hay 2012), and ecosystem biomes (Huang *et al* 2019). In most satellite-based LUE GPP models, T_s has been defined as a function of T_{opt}, maximum temperature, and minimum temperature for vegetation growth. As reported, the temperature scalar (T_s) is more sensitive and is more highly governed by the choice of T_{opt} than by maximum and minimum temperatures (Raich *et al* 1991; Zhang *et al* 2017b). Thus, the choice of T_{opt} largely affects the T_s and finally affects the accuracy of GPP estimates in the models.

Biome-specific optimum air temperature parameters (T_{opt-b}) have been used to calculate biome-specific temperature scalars (T_{s-b}) in biogeochemical models (table S1), including the Moderate Resolution Imaging Spectro-radiometer (MODIS) GPP algorithm (Running and Zhao 2015), Vegetation Photosynthesis Model (VPM; Xiao *et al* 2004b), TEC (Yan *et al* 2015), C-Fix (Veroustraete *et al* 2002), EC-LUE (Yuan *et al* 2007), CFLUX (King *et al* 2011), and GLO-PEM (Prince and Goward 1995). Several studies have reported that the use of biome-specific parameters introduced an inaccurate derivation of ε and could be one of the potential error sources in GPP data product (Heinsch *et al* 2006; Turner *et al* 2006; Sjöström *et al* 2013). Note that a vegetation biome often covers a very large geographical domain, and vegetation may adapt to its local climate over years and thus develop a site-specific optimum air temperature (T_{opt-s}) (Huang *et al* 2019). There is a need to quantify the range of T_{opt-s} parameter values and the difference between the T_{opt-s} and T_{opt-b} parameters. There is also a need to quantify the potential of using the T_{opt-s} parameter to improve GPP estimates in the models. To date, only a few studies have reported the use of T_{opt-s} in estimating GPP (Potter *et al* 2003, Sasai *et al* 2005). However, these studies have not used the GPP estimates and air temperature from the eddy flux tower sites to quantify the relationship between air temperature and GPP and estimate T_{opt-s} parameter values. Therefore, our knowledge of the T_{opt-s} parameter values and the potential of using the T_{opt-s} parameter to improve GPP estimates is still very limited. A number of scientific questions need to be addressed: what is the most appropriate method for estimating T_{opt-s} from both GPP data in the eddy flux tower sites (GPP_{EC}) and satellite datasets (NDVI, EVI)? What are the differences between site-specific temperature scalar (T_{s-s}) and biome-specific temperature scalar (T_{s-b}), and to what degree does T_{opt-s} affect GPP estimates in the data-driven models? The answers to these questions will help improve our understanding of many aspects of terrestrial carbon cycling, such as the impacts of climatic extremes (e.g. heatwave, cold spill) on the seasonal dynamics and inter-annual variation of GPP.

Grasslands in mid- to high-latitude regions are sensitive and vulnerable to climate variability, and temperature is a major climate factor controlling GPP (Yi *et al* 2010). Also grasslands have the largest inter-annual variation of gross and net primary production among the major ecosystem types (Fridley *et al* 2016; Hufkens *et al* 2016; Knapp *et al* 2017). Grasslands in these regions have high uncertainties in satellite-based GPP estimates. Compared with *in situ* flux observations, studies have found that the MOD17 GPP algorithm underestimated grassland GPP from sites to regions (Doughty *et al* 2018; Zhu *et al* 2016; Zhu *et al* 2018). The VPM GPP product added a C3/C4 ratio for the parameter ε calculation and significantly improved grassland GPP estimates (Zhang *et al* 2017b). However, larger uncertainties still exist in mid- to high-latitude grassland VPM GPP estimates (Wu *et al* 2018). The large uncertainties in grassland GPP estimates directly hinder our understanding of inner- and inter-annual GPP dynamics, and affect our assessment of ecosystem response to climate variability. For example, an analysis using MOD17 GPP showed large carbon losses for the US in 2012 because of the warm spring and dry summer (Wolf *et al* 2016), while the VPM GPP showed a slight carbon uptake (Wu *et al* 2018). In this study, first we quantified T_{opt-s} parameter values in 11 grassland sites in mid- to high-latitude regions, and compared the T_{opt-s} and T_{opt-b} parameters. Our hypothesis is that the T_{opt-s} parameter for photosynthesis of mid- to high-latitude grasslands varies among the sites and differs substantially from the commonly used T_{opt-b}. In order to explore the effects of the methods that are used to estimate T_{opt-s}, and identify potential data sources for T_{opt-s} calculation across the globe, T_{opt-s} values were calculated and compared with multiple data sources (GPP_{EC}, MODIS NDVI, and EVI) and different methods. Second, we assessed the effects of the T_{opt-s} parameter on GPP estimates in these grasslands sites. Our hypothesis is that the T_{opt-b} parameter value may result in a large overestimation or underestimation of GPP of grasslands in previous GPP products, depending upon the differences between T_{opt-s} at individual sites and T_{opt-b}. The VPM, which was developed under the LUE concept and satellite datasets (Xiao *et al* 2004b;

Zhang *et al* 2017b), was used to estimate GPP for each site over several years. We also estimated and compared VPM GPP products driven by the two different types of T_s, including both T_{s-s} (GPP_s) and T_{s-b} (GPP_b). The results from this study may help improve T_{opt-s} parameter estimates and GPP estimates in the grasslands.

2. Materials and methods

2.1. Study sites

Data from grassland flux tower sites at mid- to high-latitudes were used in this study, and the details for these sites are described in the FLUXNET-2015 dataset. We selected the flux sites based on the following criteria: (1) the site has obvious seasonal changes, winter (daily daytime mean temperature (T_{DT}) lower than 0 °C) lasting at least 2 months for each year; (2) land cover type at the site is homogeneous within the MOD09A1 (500 m) pixel (figure S1); (3) the site has had continuous observation for at least 1 year. In this study, we selected and analyzed 11 grassland sites. Spatial distribution and meteorological information of all the flux tower sites used in the analysis are shown in figure S2 and table S2.

2.2. Meteorological data and GPP data from the flux tower sites

The FLUXNET-2015 dataset provides meteorological data, water flux, and CO_2 flux data at half-hourly, hourly, daily, and yearly intervals. We visually checked the tower observations, and the values with low quality such as those with the same values in a whole year were removed. We also calculated daily downward surface solar shortwave radiation ($s_{s\downarrow}$), daily daytime mean temperature (T_{DT}), and daily GPP (GPP_{EC}) which were calculated with the variable USTAR filtering approach and daytime portioning method (Kumar *et al* 2016). Then, 8 day $s_{s\downarrow}$, T_{DT} and GPP_{EC} were generated from daily products respectively, and used in the VPM GPP simulation and comparison.

2.3. MODIS vegetation indices

This study used the MODIS land reflectance product MOD09A1 V006 (500 m spatial resolution and 8 day intervals) (Vermote 2015). For all the sites, three vegetation indices including the normalized difference vegetation index (NDVI) (Rouse Jr *et al* 1974; Chang *et al* 2018), enhanced vegetation index (EVI; Huete *et al* 2002), and land surface water index (LSWI) (Xiao *et al* 2004a) were calculated using equations (1)–(3) based on the following MODIS spectral bands: red band (RED) (620–670 nm); near infrared band (NIR) (841–876 nm); blue band (BLUE) (459–479 nm), green band (GREEN) (545–565 nm), and short wavelength near infrared band (SWIR) (1628–1652 nm).

$$\mathrm{NDVI} = \frac{\mathrm{NIR} - \mathrm{RED}}{\mathrm{NIR} + \mathrm{RED}} \tag{1}$$

$$\mathrm{EVI} = 2.5 \times \frac{\mathrm{NIR} - \mathrm{RED}}{(\mathrm{NIR} + 6 \times \mathrm{RED} - 7.5 \times \mathrm{BLUE} + 1)} \tag{2}$$

$$\mathrm{LSWI} = \frac{\mathrm{NIR} - \mathrm{SWIR}}{\mathrm{NIR} + \mathrm{SWIR}}. \tag{3}$$

To filter out poor quality observations, we firstly identified those affected by ice, snow, and clouds using the quality control (QC) layer (Zhang *et al* 2017b). Poor quality observations were replaced by the multi-year mean of good observations during the same time period. The Best Index Slope Extraction method was used to further detect the abnormal observations unidentified by the QC layer. The abnormal values were then filled with the mean value of its nearest two observations (Viovy *et al* 1992; White *et al* 1997, Xiao *et al* 2009). At the end, the Savitzky–Golay (S–G) filter model was designed for removing the existing abnormal values (Savitzky and Golay 1964; Chen *et al* 2004).

2.4. Methods for estimating site-specific optimum temperature for GPP

Biome-specific optimum air temperature (T_{opt-b}) was used at 27 °C as reported in the global VPM GPP product (Zhang *et al* 2017b). Site-specific optimum air temperature (T_{opt-s}) was estimated from the analyses of temperature, GPP_{EC}, EVI, and NDVI data at individual flux tower sites. We developed two new methods to estimate T_{opt-s}, namely, the 95% maximum method and the generalized additive model (GAM) regression method. In order to make a comparison with a previous study (Potter *et al* 2003), we also estimated the T_{opt-s} from NDVI following the method in the CASA model, which is denoted as $T_{opt-s-CASA-NDVI}$. In the response curve between the daily air temperature (*x*-axis) and GPP or vegetation indices (*y*-axis) (figure 1), we define the site-specific optimum air temperature as the daily air temperature when GPP or vegetation indices reach their peak value within the growing season.

With the 95% maximum method, we firstly found the maximum values of GPP_{EC} ($GPP_{EC\text{-}max}$), or EVI (EVI_{max}), for each site. We calculated the optimum temperature as the daily daytime mean temperature (T_{DT}) during those observations with GPP or EVI values equal to or higher than 95% $GPP_{EC\text{-}max}$ or EVI_{max} (figures 1(a) and (b)). Estimated T_{opt-s} using the 95% maximum method from GPP_{EC} and EVI are denoted as $T_{opt-s-95-GPP_{EC}}$, $T_{opt-s-95-EVI}$. Following the CASA model and NDVI, the $T_{opt-s-CASA-NDVI}$ was defined as the average monthly T_{DT} when $GPP_{EC\text{-}max}$ or EVI_{max} occurred (figure 1(c)).

With the GAM regression method, the relationship between the GPP_{EC} values (or EVI values) and the T_{DT} at a site over all the years were determined using a cyclic penalized cubic regression spline smooth model in R software. The optimum temperature for this site was then defined as the T_{DT} when GPP_{EC} (or EVI) reached the maximum value in the GAM regression line (figures 1(d), (e)). T_{opt-s} estimated by the GAM

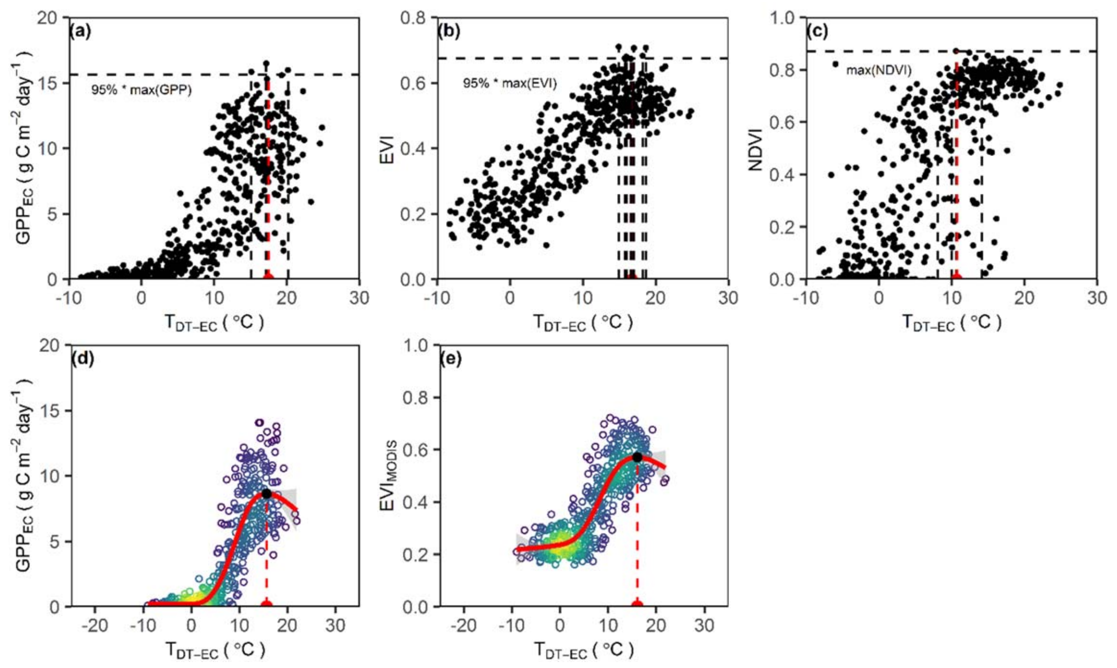

Figure 1. Methods used for estimating site-specific optimum air temperature (T_{opt-s}) at AT-Neu. (a) and (b) T_{opt-s} was defined with the 95% maximum method from the GPP_{EC} and EVI; (c) T_{opt-s} was defined with the CASA averaged monthly method from the NDVI; (d) and (e) T_{opt-s} was defined with the GAM regression method from the GPP_{EC} and EVI. The black dashed lines represent the selected observations for the T_{opt-s} calculations. The red dashed lines and points represent the T_{opt-s} results.

method from GPP_{EC} and EVI are denoted as $T_{opt-s-GAM-GPP_{EC}}$, and $T_{opt-s-GAM-EVI}$.

2.5. GPP simulation by the VPM model

The VPM estimates daily GPP (GPP_{VPM}), is driven by satellite images and climate data (Xiao *et al* 2004b), and has been widely used in GPP simulation at site, regional, and global scales (Zhang *et al* 2017b; Wu *et al* 2018; Chang *et al* 2019). In the VPM model, daily GPP is estimated by APAR by chlorophyll in the canopy ($APAR_{chl}$; $APAR_{chl} = FPAR_{chl} * PAR$) and LUE ($\varepsilon$), see equations (4) and (5):

$$GPP_{VPM} = \varepsilon \times FPAR_{chl} \times PAR \quad (4)$$

$$\varepsilon = \varepsilon_0 \times T_s \times W_s \quad (5)$$

where ε is LUE, $FPAR_{chl}$ is the fraction of PAR absorbed by chlorophyll, and PAR is the photosynthetic active radiation. EVI is used to estimate $FPAR_{chl}$. Temperature stress (T_s) and water stress (W_s) are used to downscale maximum LUE (ε_0) and estimate ε.

T_s is calculated using the temperature response equation documented in the Terrestrial Ecosystem Model (Raich *et al* (1991)), as shown in equation (6):

$$T_s = \frac{(T - T_{min})(T - T_{max})}{(T - T_{min})(T - T_{max}) - (T - T_{opt})^2} \quad (6)$$

where T is the daily daytime mean air temperature (°C); T_{min}, T_{max}, and T_{opt} are the minimum, maximum, and maximum air temperatures for photosynthesis, respectively. The biome-specific parameters used in the global VPM GPP simulations came from the biome-specific look-up table, and the T_{opt} for grasslands was set as 27 °C (Zhang *et al* 2017b). Four groups of site-specific T_s (T_{s-s}) were calculated using the two methods (95% max and GAM) from GPP_{EC} and EVI, and are denoted as $T_{s-s-95-GPP_{EC}}$, $T_{s-s-95-EVI}$, $T_{s-s-GAM-GPP_{EC}}$, and $Ts{-}s{-}GAM{-}EVI$ and the four groups of GPP_{VPM} based on T_{s-s} are denoted as $GPP_{VPM-s-95-GPP_{EC}}$, $GPP_{VPM-s-95-EVI}$, $GPP_{VPM-s-GAM-GPP_{EC}}$, and $GPP_{VPM-s-GAM-EVI}$.

3. Results

3.1. Estimation of site-specific optimum air temperature from GPP_{EC} and vegetation index

We estimated T_{opt-s} for each site with the three methods using GPP_{EC}, EVI, and NDVI (table S2). The results (figure 2) showed that the T_{opt-s} values showed a large difference within the grassland sites, and the estimates of T_{opt-s} for individual sites were very different form the T_{opt-b} used in the global VPM GPP product (27 °C). For the estimates of T_{opt-s} based on every method, the difference between the highest and lowest T_{opt-s} of the 11 grassland sites was larger than 10 °C. T_{opt-s} calculated from EVI and NDVI were significantly correlated with T_{opt-s} from GPP_{EC} when using same estimation method (root mean square error (RMSE) values are from 1.58–3.28 °C). As shown by the linear regression results (RMSE, R^2, P-value), T_{opt-s} estimates from NDVI using the two methods developed in our study, $T_{opt-s-95-NDVI}$ and $T_{opt-s-GAM-NDVI}$,

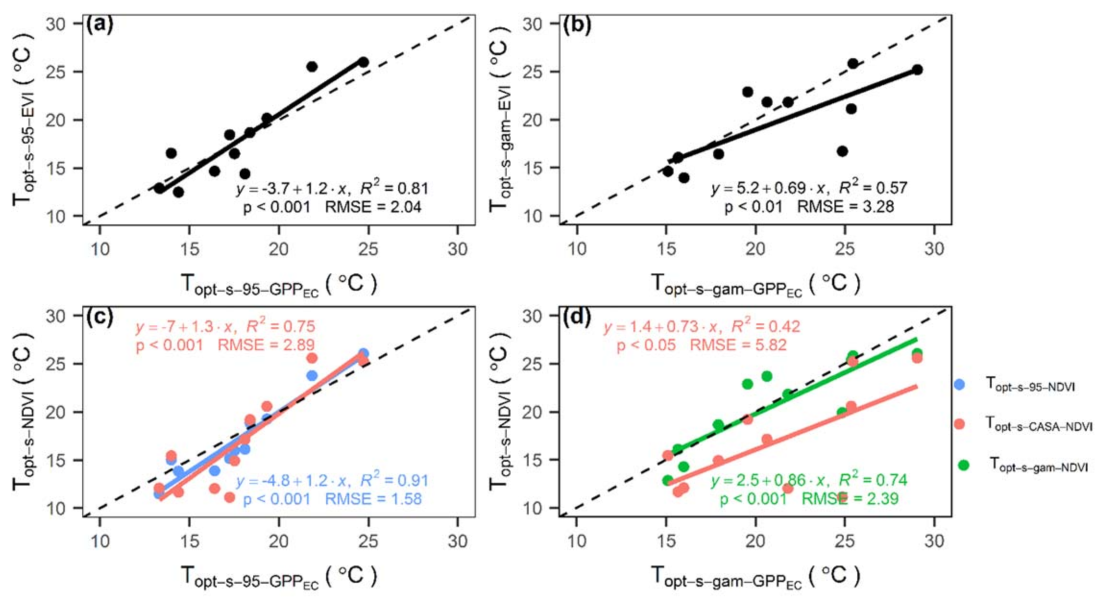

Figure 2. Comparisons among site-specific optimum temperature ($T_{\mathrm{opt-s}}$) values estimated with different methods and data sources. $T_{\mathrm{opt-s-95-GPP_{EC}}}$, $T_{\mathrm{opt-s-95-EVI}}$, and $T_{\mathrm{opt-s-95-NDVI}}$ are the $T_{\mathrm{opt-s}}$ from eddy covariance GPP ($\mathrm{GPP_{EC}}$), MODIS EVI, and NDVI using the 95% maximum method; $T_{\mathrm{opt-s-GAM-GPP_{EC}}}$, $T_{\mathrm{opt-s-GAM-EVI}}$, and $T_{\mathrm{opt-s-GAM-NDVI}}$ are the $T_{\mathrm{opt-s}}$ from eddy covariance $\mathrm{GPP_{EC}}$, EVI, and NDVI using the GAM regression method. $T_{\mathrm{opt-s-CASA-NDVI}}$ is the $T_{\mathrm{opt-s}}$ calculated from NDVI following the CASA model. Solid lines are linear regression lines.

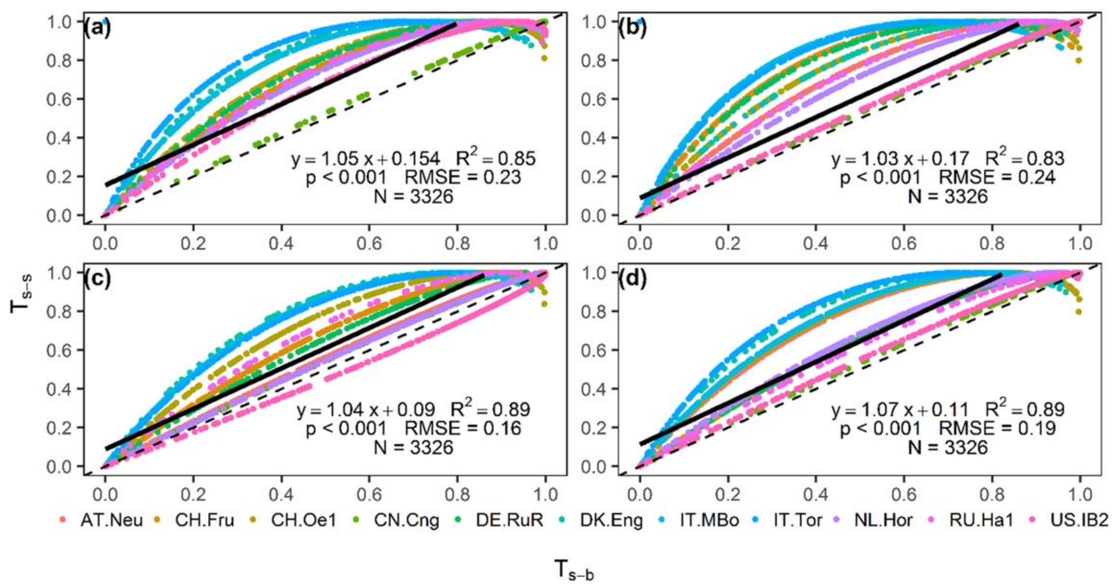

Figure 3. Comparison of site-specific temperature scalar ($T_{\mathrm{s-s}}$) values and biome-specific temperature scalar ($T_{\mathrm{s-b}}$) for all grassland sites. (a) $T_{\mathrm{s-s-95-GPP_{EC}}}$ and (b) $T_{\mathrm{s-s-95-EVI}}$ are from eddy covariance GPP ($\mathrm{GPP_{EC}}$) and EVI with the 95% maximum method; (c) $T_{\mathrm{s-s-GAM-GPP_{EC}}}$ and (d) $T_{\mathrm{s-s-GAM-EVI}}$ are the $T_{\mathrm{s-s}}$ from eddy covariance GPP ($\mathrm{GPP_{EC}}$) and EVI with the GAM regression method. The black line in each panel is a linear regression line for all samples. Other colors represent different flux tower sites.

were more consistent with $T_{\mathrm{opt-s}}$ estimates from $\mathrm{GPP_{EC}}$ ($T_{\mathrm{opt-s-GPP_{EC}}}$) than those from the CASA model ($T_{\mathrm{opt-s-CASA-NDVI}}$) (figures 2(c) and (d)).

3.2. Effects of site-specific optimum air temperature on temperature scalars in the models

$T_{\mathrm{opt-s}}$ based $T_{\mathrm{s-s}}$ values in the VPM model were calculated with $T_{\mathrm{opt-s-95-GPP_{EC}}}$, $T_{\mathrm{opt-s-95-EVI}}$, $T_{\mathrm{opt-s-GAM-GPP_{EC}}}$, and $T_{\mathrm{opt-s-GAM-EVI}}$. The results showed that the $T_{\mathrm{s-s}}$ values in the model for all observations at the 11 sites (figure 3) have large differences from $T_{\mathrm{s-b}}$, and most of the $T_{\mathrm{s-s}}$ values were larger than $T_{\mathrm{s-b}}$. The results indicated that the use of $T_{\mathrm{s-b}}$ in a previous global GPP simulation had underestimated T_s or overestimated the temperature limitation (temperature constraints) on the photosynthesis of grassland sites, especially for the sites with low temperatures such as IT-Tor and IT-MBo, where the annual mean temperatures are 5.1 °C and 2.9 °C, respectively (table S3).

Table 1. A comparison between GPP_{VPM} calculated with T_{s-s} (GPP_{VPM-s}), T_{s-b} (GPP_{VPM-b}), and GPP_{EC}. Simple linear regression models were used at each eddy covariance site, and R^2 and RMSE ($g\,C/m^2/day$) were shown. *** means a P-value less than 0.001.

SiteID	Cor (GPP_{VPM-b}, GPP_{EC})	Cor ($GPP_{VPM-s-95-GPP_{EC}}$, GPP_{EC})	Cor ($GPP_{VPM-s-95-EVI}$, GPP_{EC})	Cor ($GPP_{VPM-s-GAM-GPP_{EC}}$, GPP_{EC})	Cor ($GPP_{VPM-s-GAM-EVI}$, GPP_{EC})
AT-Neu	0.75^{***},3.02	0.80^{***},2.38	0.80^{***},2.37	0.76^{***},2.81	0.80^{***},2.31
CH-Fru	0.76^{***},2.79	0.81^{***},2.18	0.82^{***},2.02	0.79^{***},2.30	0.79^{***},2.37
CH-Oe1	0.47^{***},3.72	0.52^{***},3.28	0.52^{***},3.27	0.52^{***},3.30	0.52^{***},3.27
CN-Cng	0.85^{***},1.06	0.85^{***},1.04	0.85^{***},1.04	0.85^{***},1.04	0.85^{***},1.04
DE-RuR	0.81^{***},1.89	0.85^{***},1.77	0.86^{***},1.75	0.83^{***},1.73	0.83^{***},1.73
DK-Eng	0.37^{***},2.59	0.43^{***},2.83	0.42^{***},2.88	0.43^{***},2.86	0.43^{***},2.85
IT-MBo	0.83^{***},1.75	0.89^{***},1.76	0.89^{***},1.74	0.88^{***},1.75	0.88^{***},1.75
IT-Tor	0.89^{***},1.31	0.91^{***},1.60	0.91^{***},1.58	0.91^{***},1.43	0.91^{***},1.54
NL-Hor	0.82^{***},1.71	0.83^{***},2.00	0.83^{***},1.99	0.82^{***},1.79	0.83^{***},1.97
RU-Ha1	0.85^{***},1.15	0.87^{***},0.991	0.87^{***},0.99	0.86^{***},1.00	0.86^{***},1.04
US-IB2	0.84^{***},1.76	0.86^{***},1.65	0.84^{***},1.75	0.83^{***},1.77	0.84^{***},1.74

3.3. Effects of site-specific temperature scalar on GPP estimates in the model simulation

For most grassland sites, GPP_{VPM} values calculated with T_{s-s} (GPP_{VPM-s}) were significantly correlated with GPP_{EC}, and had a higher correlation coefficient (R^2) and lower RMSE than results from GPP_{VPM-b} (table 1). Also, GPP_{VPM-s} values estimated from four types of T_{s-s} ($T_{s-s-95-GPP_{EC}}$, $T_{s-s-95-EVI}$, $T_{s-s-GAM-GPP_{EC}}$, and $T_{s-s-GAM-EVI}$) were higher than GPP_{VPM-b} with various values for almost all the intervals of the total 11 grassland sites (figures 4(a)–(d)). For some sites, the GPP_{VPM-s} values were higher than GPP_{VPM-b}, up to 4 g C m^{-2} day^{-1} in the summer. In addition, the average annual GPP_{VPM-b} (1121.20 g C m^{-2} $year^{-1}$) was 25.36% lower than the average annual GPP_{EC} for the selected grassland sites (1502.16 g C m^{-2} $year^{-1}$) (figure 4(e)). The average annual GPP_{VPM-s} was higher than GPP_{VPM-b} for 80∼178 g C m^{-2} $year^{-1}$, depending upon the method. Four types of annual GPP_{VPM-s} were lower than GPP_{EC} for 11.95% ($GPP_{VPM-s-GAM-GPP_{EC}}$), 8.00% ($GPP_{VPM-s-GAM-GPP_{EC}}$), 5.81% ($GPP_{VPM-s-95-GPP_{EC}}$), and 5.35% ($GPP_{VPM-s-95-EVI}$) respectively. Similarly, RMSE values between the four GPP_{VPM-s} and GPP_{EC} were lower than that between GPP_{VPM-b} and GPP_{EC}. From both 8 day and annual analyses, the results indicated that using a site-specific optimum temperature improved the accuracy of the GPP estimates in the VPM model.

4. Discussion

T_{opt} was generally studied and estimated along the level of organization of species, community, and ecosystem. The studies indicated that T_{opt} varies across species and across ecosystems (biomes) (Kattge and Knorr 2007; Lin *et al* 2012), and T_{opt-b} was used in the biogeochemical models. Different from most previous studies, our study explored and discussed the variability of T_{opt} across sites within a biome. Our results showed large differences of T_{opt} across sites within a biome, and thus supported the urgent need to address T_{opt-s} in a global terrestrial ecosystem study. In addition, the ecosystem-level T_{opt-b} parameters in previous global process-based ecosystem models were directly scaled from the leaf-level T_{opt-b} parameters, in which the T_{opt-b} values at the ecosystem level were found to be consistently lower than those at the leaf level and varied spatially (Huang *et al* 2019). Our study introduced the methods by using satellite datasets for ecosystem-level T_{opt-s} extraction. The new methods provide a new way and results for future ecosystem T_{opt} studies. Previous studies have suggested gradually changed T_{opt} values along the latitude, while our study did not find a clear relationship between T_{opt} and latitude, annual precipitation, and temperature for the 11 grassland sites (figure S3). This is likely caused by the limited number of grassland sites, or due to grasslands being sensitive to both temperature anomalies and water supply and cannot be well explained by a single climate factor (Hufkens *et al* 2016; Green *et al* 2019).

In recent years, many approaches have been developed to reduce the impacts from biome-specific look-up table parameters and coarse image resolutions in GPP estimates, such as readjusting biome-specific parameters (Sjöström *et al* 2013), considering different C3/C4 ε_0 values (Zhang *et al* 2017b; Wu *et al* 2018), and generating new equations for LUE (Ma *et al* 2014). Our study contributed the LUE estimates by adjusting the temperature parameter and therefore temperature scalars, which was a less considered direction. Even though the CASA model has already tried to use T_{opt-s} instead of T_{opt-b} in the Net Photosynthesis Productivity (NPP) products (Field *et al* 1995), the two methods (95% max and GAM regression) developed in our study improved the estimates of T_{opt-s}, significantly. Compared with the T_{opt-s} estimated from NDVI in the CASA model, T_{opt-s} estimated from EVI was more consistent to T_{opt-s} from GPP_{EC} (figure 2), which indicates that EVI is a reliable indicator for T_{opt-s} estimation in space, which could contribute to a

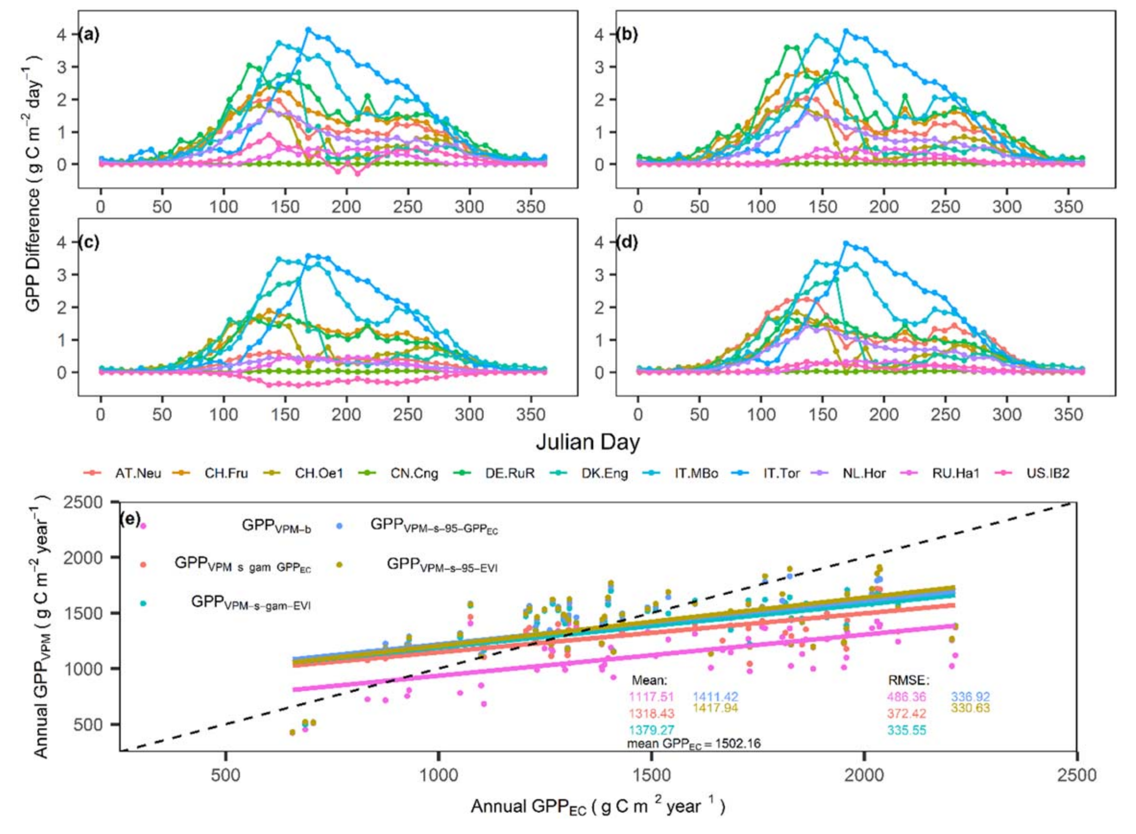

Figure 4. Seasonal and annual comparisons among modeled GPP_{VPM} values and GPP_{EC}. (a)–(d) Seasonal characteristics for values of the difference between GPP_{VPM} with the site-specific parameter (GPP_{VPM-s}) and GPP_{VPM} with the biome-specific parameter (GPP_{VPM-b}) at all grassland sites. The GPP_{VPM} are estimated at 8 day intervals. The average value for each interval is calculated for all the observation years for a single site. Four types of GPP_{VPM-s} were used: (a) $GPP_{VPM-s-95-GPPEC}$ and (b) $GPP_{VPM-s-95-EVI}$ were calculated using the T_{s-s} from eddy covariance GPP (GPP_{EC}) and EVI with the 95% maximum method; (c) $GPP_{VPM-s-GAM-GPPEC}$ and (d) $GPP_{VPM-s-GAM-EVI}$ were calculated using T_{s-s} from GPP_{EC} and EVI with the GAM regression method. The colors in (a), (b), (c), and (d) represent different flux tower sites. (e) Annual GPP_{VPM-s} and GPP_{VPM-b} compared with GPP_{EC}.

large-scale GPP simulation in the future. Because T_{opt-s} in the CASA model has usually been defined as the monthly mean temperature when NDVI reaches its maximum (Yan *et al* 2015), thus $T_{opt-s-CASA-NDVI}$ had more errors than that with a 95% max and GAM regression (figure 1). What is more, NDVI was more affected than EVI especially at regions mixed with complicated background information (Chang *et al* 2019). As a previous validation study has proved that the global GPP_{VPM} product with T_{opt-b} has been more reliable than GPP_{CASA} when compared with GOME-2 SIF data, our GPP_{VPM} with T_{opt-s} could be much more competitive in model comparison studies (Wu *et al* 2018). It is important to apply the T_{opt-s} estimation methods in other land cover types, and explore the effects on GPP simulation. Both the datasets and methods in this study have widely applicability in other land cover types.

Accurate T_{opt-s} estimation is a reasonably reliable way for improving GPP estimates. A CASA model research study improved NPP by about 50 g C m^{-2} yr^{-1} at China's Shennongjia Forestry District in the Hubei province by slightly improving the T_{opt-s} estimation method, in which the T_{opt-s} was defined as the mean temperature during the period of mature stability (Pei *et al* 2018). Our results indicated that using T_{opt-b} in previous VPM GPP studies could lead to an underestimation of GPP of 25% for grassland ecosystems annually (figure 4(e)). But we found that even though the use of T_{opt-s} improved GPP estimation and resulted in higher GPP values than using T_{opt-b} in most grassland sites, GPP_{VPM} with T_{opt-s} was still lower than GPP_{EC} from eddy covariance observation for many of the 8 day intervals (figures S4(a)–(d)), and GPP_{VPM-s} was about 5%–12% lower than GPP_{EC} annually (figure 4(e)). The annual underestimation mostly occurred in the higher GPP years with 1400 g C m^{-2} yr^{-1} at AT-Neu (2002–2012) and CH-Oe1 (2002–2007), which could be caused by the inter-annual and inner-annual variability of C3/C4 composition which are not well recognized in the models (Doughty *et al* 2018; Zhu *et al* 2018). Åt AT-Neu (figure S6) and CH-Oe1 (figure S7), the start of the season and end of the season from GPP_{EC} and GPP_{VPM} agrees well with each other, but the magnitude differs substantially between them within a few years (e.g. 2002, 2003, 2004, 2006 at AT-Neu). Both shortwave radiation data and vegetation index data do not support a very high GPP_{EC} during the 8 day periods of those years. We used daily GPP portioned by net ecosystem exchange (NEE) in the flux tower sites which has been reported to have errors or uncertainties in some observations (Reichstein *et al* 2005). Here, we would like to attribute the quality of GPP_{EC} data as a major source of the large discrepancy between annual GPP_{VPM} and GPP_{EC} in some years. The daily GPP data showed that the abnormal GPP_{EC} values could be caused by the intensive rainfall (figures S8 and S9). The consistency between GPP_{EC} and climate data and remote sensing data is important for us to evaluate GPP_{EC} data. However, the use of T_{opt-s} was slightly overestimated for the years with lower annual GPP. The overestimation for low GPP years, mostly occurred at IT-Tor (2009–2013), and could be related to the water stress or lower annual precipitation in these years (628–818 mm yr^{-1}) relative to the multi-year mean annual precipitation (920 mm yr^{-1}). Under drought conditions, there could be a lower T_{opt-s} than in normal years. Further studies are needed to explore the possible ways to improve GPP estimation at the ecosystem scale. Other likely sources of uncertainty in data-driven GPP products include for example the model structure (Zheng *et al* 2018), meteorological input datasets (Anav *et al* 2015), and seasonal dynamic of LUE (Wei *et al* 2017). Many novel approaches have been developed to reduce uncertainties in GPP estimates. For example, a study estimated GPP by only using PAR and EVI (Ma *et al* 2014). The Photochemical Reflectance Index was found to be significantly correlated to LUE, and was effective in detecting seasonal carbon fluxes in evergreen ecosystems where FPAR and greenness-related vegetation indices change little (Garbulsky *et al* 2011; Middleton *et al* 2016). NIRv was better correlated to modeled MODIS FPAR than NDVI and significantly correlated to GPP (Badgley *et al* 2017), and has been used for GPP estimates globally in 0.5° (Badgley *et al* 2018). Also, significant linear relationships between GPP and OCO-2-based SIF product (GOSIF) contributed to the work that estimated GPP in 0.05° using GOSIF (Li and Xiao 2019). Further studies are needed to explore the possible ways to improve GPP estimation at the ecosystem scale.

The satellite-based GPP_{VPM-s} product with higher estimate accuracies could be more reliable for studying the impacts of climate variability, especially extreme climate events, on the ecosystem. Here, we take drought, which is expected to show an intensified frequency and consequences under climate change (Jiao *et al* 2016; Jiao *et al* 2019b), as an example for discussing the possible contributions of our study in a future study. Previous studies based on three different global GPP products reported that the impact of drought on terrestrial primary production was underestimated by satellite-based LUE GPP models (Turner *et al* 2005; Mu *et al* 2007; Sims *et al* 2008). The reason for the underestimation is that these GPP models did not simulate the water balance, or did not account for the direct effects of soil moisture in addition to VPD and changes in greenness (Jiao *et al* 2019a; Stocker *et al* 2019). Our study found that GPP_{VPM} computed with T_{opt-s} for the years with higher precipitation showed a greater improvement than for the years with lower precipitation (figure S5). This result indicated that the T_{opt-b} used in previous global GPP simulations might finally underestimate the decrease of GPP from a normal year to a drought year, which could be one of the reasons for the underestimation of drought impacts on ecosystem productivity. As known, when drought occurs, it is often accompanied by higher temperature (Zhang *et al* 2017a). The plants thus actually suffer both water stress and temperature stress under drought. As the drought condition T_{opt-s} was different with and lower than T_{opt-b}, the use of T_{opt-b} might not capture well the effect of increasing temperature on GPP, and therefore resulted in a greater underestimation. Future GPP models need to consider the comprehensive impacts from multi-parameters such as temperature, water, canopy structural, leaf nitrogen, and chlorophyll content.

5. Conclusions

Our study explored the estimates of T_{opt-s} using a satellite and the potential of using T_{opt-s} in estimating the GPP of grasslands. We found that EVI has a similar performance with *in situ* measured GPP_{EC} for determining photosynthesis T_{opt-s}. We also compared the differences in T_{opt-s} values using different extraction methods and different data sources. Our results provide references with data sources and methods for reliable T_{opt-s} estimation and more accurate GPP simulations at the site and global scales. T_{opt-s} values differ among sites and differ from T_{opt-b} significantly. We found a significant improvement in the accuracy of GPP estimates for grasslands by using T_{opt-s} rather than T_{opt-b}. We suggest that terrestrial ecosystem models should account for site-specific temperature parameters. As the climatic impacts on ecosystems have always been assessed by GPP anomalies, an improved GPP product would help us better understand the impacts of extreme events on terrestrial ecosystem carbon cycles, and better manage terrestrial ecosystems.

Acknowledgments

This study was supported by research grants from the USDA National Institute of Food and Agriculture (NIFA) (2013-69002 and 2016-68002-24967) and the US National Science Foundation EPSCoR program (IIA-1301789). This work used eddy covariance data acquired and shared by the FLUXNET community, including these networks: AmeriFlux, AfriFlux, AsiaFlux, CarboAfrica, CarboEuropeIP, CarboItaly, CarboMont, ChinaFlux, Fluxnet-Canada, GreenGrass, ICOS, KoFlux, LBA, NECC, OzFlux-TERN, TCOS-Siberia, and USCCC. The FLUXNET-2015 dataset can be downloaded from http://fluxnet.fluxdata.org/data/fluxnet2015-dataset/. All the other datasets used in this study are discussed in section 2.

Data availability

Any data that support the findings of this study are included and discussed within the article.

ORCID iDs

Yuanwei Qin https://orcid.org/0000-0002-5181-9986

References

Anav A, Friedlingstein P, Beer C, Ciais P, Harper A, Jones C, Murray-Tortarolo G, Papale D, Parazoo N C and Peylin P 2015 Spatiotemporal patterns of terrestrial gross primary production: a review *Rev. Geophys.* **53** 785–818

Badgley G, Field C B and Berry J A 2017 Canopy near-infrared reflectance and terrestrial photosynthesis *Sci. Adv.* **3** e1602244

Badgley G, Anderegg L D, Berry J A and Field C B 2018 Terrestrial gross primary production: using NIRV to scale from site to globe *Glob. Change Biol.* **25** 3731–40

Battaglia M, Beadle C and Loughhead S 1996 Photosynthetic temperature responses of *Eucalyptus globulus* and *Eucalyptus nitens Tree Physiol.* **16** 81–9

Berry J and Bjorkman O 1980 Photosynthetic response and adaptation to temperature in higher plants *Ann. Rev. Plant Physiol.* **31** 491–543

Chang Q, Zhang J, Jiao W and Yao F 2018 A comparative analysis of the NDVIg and NDVI3g in monitoring vegetation phenology changes in the Northern Hemisphere *Geocarto Int.* **33** 1–20

Chang Q, Xiao X, Jiao W, Wu X, Doughty R, Wang J, Du L, Zou Z and Qin Y 2019 Assessing consistency of spring phenology of snow-covered forests as estimated by vegetation indices, gross primary production, and solar-induced chlorophyll fluorescence *Agric. For. Meteorol.* **275** 305–16

Chen J, Jönsson P, Tamura M, Gu Z, Matsushita B and Eklundh L 2004 A simple method for reconstructing a high-quality NDVI time-series data set based on the Savitzky–Golay filter *Remote Sens. Environ.* **91** 332–44

Clark D, Mercado L, Sitch S, Jones C, Gedney N, Best M, Pryor M, Rooney G, Essery R and Blyth E 2011 The Joint UK Land Environment Simulator (JULES), model description: II. Carbon fluxes and vegetation dynamics *Geosci. Model Dev.* **4** 701–22

Cox P M 2001 Description of the' TRIFFID' dynamic global vegetation model *Technical Note 24* Hadley Centre (https://pdfs.semanticscholar.org/b214/624cfd3764c091804c73ed213d4f85f03cba.pdf)

Doughty R, Xiao X, Wu X, Zhang Y, Bajgain R, Zhou Y, Qin Y, Zou Z, McCarthy H and Friedman J 2018 Responses of gross primary production of grasslands and croplands under drought, pluvial, and irrigation conditions during 2010–2016, Oklahoma, USA *Agric. Water Manage.* **204** 47–59

Field C B, Randerson J T and Malmström C M 1995 Global net primary production: combining ecology and remote sensing *Remote Sens. Environ.* **51** 74–88

Fitter A H and Hay R K 2012 *Environmental Physiology of Plants* (New York: Academic)

Fridley J D, Lynn J S, Grime J and Askew A 2016 Longer growing seasons shift grassland vegetation towards more-productive species *Nat. Clim. Change* **6** 865

Garbulsky M F, Peñuelas J, Gamon J, Inoue Y and Filella I 2011 The photochemical reflectance index (PRI) and the remote sensing of leaf, canopy and ecosystem radiation use efficiencies: a review and meta-analysis *Remote Sens. Environ.* **115** 281–97

Green J K, Seneviratne S I, Berg A M, Findell K L, Hagemann S, Lawrence D M and Gentine P 2019 Large influence of soil moisture on long-term terrestrial carbon uptake *Nature* **565** 476

Heinsch F A, Zhao M, Running S W, Kimball J S, Nemani R R, Davis K J, Bolstad P V, Cook B D, Desai A R and Ricciuto D M 2006 Evaluation of remote sensing based terrestrial productivity from MODIS using regional tower eddy flux network observations *IEEE Trans. Geosci. Remote Sens.* **44** 1908–25

Huang M, Piao S, Ciais P, Peñuelas J, Wang X, Keenan T F, Peng S, Berry J A, Wang K and Mao J 2019 Air temperature optima of vegetation productivity across global biomes *Nat. Ecol. Evol.* **3** 772–9

Huete A, Didan K, Miura T, Rodriguez E P, Gao X and Ferreira L G 2002 Overview of the radiometric and biophysical performance of the MODIS vegetation indices *Remote Sens. Environ.* **83** 195–213

Hufkens K, Keenan T F, Flanagan L B, Scott R L, Bernacchi C J, Joo E, Brunsell N A, Verfaillie J and Richardson A D 2016 Productivity of North American grasslands is increased under future climate scenarios despite rising aridity *Nat. Clim. Change* **6** 710

Jiang C and Ryu Y 2016 Multi-scale evaluation of global gross primary productivity and evapotranspiration products derived from Breathing Earth System Simulator (BESS) *Remote Sens. Environ.* **186** 528–47

Jiao W, Chang Q and Wang L 2019a The sensitivity of satellite solar-induced chlorophyll fluorescence to meteorological drought *Earth's Future* **7** 558–73

Jiao W, Tian C, Chang Q, Novick K A and Wang L 2019b A new multi-sensor integrated index for drought monitoring *Agric. For. Meteorol.* **268** 74–85

Jiao W, Zhang L, Chang Q, Fu D, Cen Y and Tong Q 2016 Evaluating an enhanced vegetation condition index (VCI) based on VIUPD for drought monitoring in the continental United States *Remote Sens.* **8** 224

Kattge J and Knorr W 2007 Temperature acclimation in a biochemical model of photosynthesis: a reanalysis of data from 36 species *Plant Cell Environ.* **30** 1176–90

King D A, Turner D P and Ritts W D 2011 Parameterization of a diagnostic carbon cycle model for continental scale application *Remote Sens. Environ.* **115** 1653–64

Kirschbaum M and Farquhar G 1984 Temperature dependence of whole-leaf photosynthesis in *Eucalyptus pauciflora* Sieb. ex Spreng *Funct. Plant Biol.* **11** 519–38

Knapp A K, Ciais P and Smith M D 2017 Reconciling inconsistencies in precipitation–productivity relationships: implications for climate change *New Phytol.* **214** 41–7

Kumar J, Hoffman F M, Hargrove W W and Collier N 2016 Understanding the representativeness of FLUXNET for upscaling carbon flux from eddy covariance measurements *Earth Syst. Sci. Data Discuss.* (https://doi.org/10.5194/essd-2016-36)

Landsberg J J 1986 *Physiological Ecology of Forest Production: Principles, Processes and Models* (London: Academic)

Li X and Xiao J 2019 Mapping photosynthesis solely from solar-induced chlorophyll fluorescence: a global, fine-resolution dataset of gross primary production derived from OCO-2 *Remote Sens.* **11** 2563

Lin Y-S, Medlyn B E and Ellsworth D S 2012 Temperature responses of leaf net photosynthesis: the role of component processes *Tree Physiol.* **32** 219–31

Ma X, Huete A, Yu Q, Restrepo-Coupe N, Beringer J, Hutley L B, Kanniah K D, Cleverly J and Eamus D 2014 Parameterization of an ecosystem light-use-efficiency model for predicting savanna GPP using MODIS EVI *Remote Sens. Environ.* **154** 253–71

McGuire A D, Melillo J M, Kicklighter D W and Joyce L A 1995 Equilibrium responses of soil carbon to climate change: empirical and process-based estimates *J. Biogeogr.* **22** 785–96

Middleton E, Huemmrich K, Landis D, Black T, Barr A and McCaughey J 2016 Photosynthetic efficiency of northern forest ecosystems using a MODIS-derived Photochemical Reflectance Index (PRI) *Remote Sens. Environ.* **187** 345–66

Monteith J L 1972 Solar radiation and productivity in tropical ecosystems *J. Appl. Ecol.* **9** 747–66
Monteith J L 1977 Climate and the efficiency of crop production in Britain *Phil. Trans. R. Soc. Lond.* B **281** 277–94
Mu Q, Zhao M and Running S W 2011 Improvements to a MODIS global terrestrial evapotranspiration algorithm *Remote Sens. Environ.* **115** 1781–800
Mu Q, Zhao M, Heinsch F A, Liu M, Tian H and Running S W 2007 Evaluating water stress controls on primary production in biogeochemical and remote sensing based models *J. Geophys. Res. Biogeosci.* **112** 1–13
Pei Y, Huang J, Wang L, Chi H and Zhao Y 2018 An improved phenology-based CASA model for estimating net primary production of forest in central China based on Landsat images *Int. J. Remote Sens.* **39** 7664–92
Potter C, Klooster S, Myneni R, Genovese V, Tan P-N and Kumar V 2003 Continental-scale comparisons of terrestrial carbon sinks estimated from satellite data and ecosystem modeling 1982–1998 *Global Planet. Change* **39** 201–13
Potter C, Randerson J, Field C, Matson P, Vitousek P, Mooney H A and Klooster S A 1993 Terrestrial ecosystem production: a process model based on global satellite and surface data *Global Biogeochem. Cycles* **7** 811–41
Prince S D and Goward S N 1995 Global primary production: a remote sensing approach *J. Biogeogr.* **22** 815–35
Raich J W, Rastetter E, Melillo J M, Kicklighter D W, Steudler P, Peterson B, Grace A, Moore B and Vorosmarty C J 1991 Potential net primary productivity in South America: application of a global model *Ecol. Appl.* **1** 399–429
Reichstein M, Falge E, Baldocchi D, Papale D, Aubinet M, Berbigier P, Bernhofer C, Buchmann N, Gilmanov T and Granier A 2005 On the separation of net ecosystem exchange into assimilation and ecosystem respiration: review and improved algorithm *Glob. Change Biol.* **11** 1424–39
Rouse J W Jr, Haas R, Schell J and Deering D 1974 Monitoring vegetation systems in the Great Plains with ERTS
Running S W and Zhao M 2015 User's Guide: Daily GPP and annual NPP (MOD17A2/A3) products NASA Earth Observing System MODIS land algorithm. Version 3.0 (https://ntsg.umt.edu/files/modis/MOD17UsersGuide2015_v3.pdf)
Ryu Y, Berry J A and Baldocchi D D 2019 What is global photosynthesis? History, uncertainties and opportunities *Remote Sens. Environ.* **223** 95–114
Sasai T, Ichii K, Yamaguchi Y and Nemani R 2005 Simulating terrestrial carbon fluxes using the new biosphere model 'biosphere model integrating eco-physiological and mechanistic approaches using satellite data'(BEAMS) *J. Geophys. Res. Biogeosci.* **110** 1–18
Savitzky A and Golay M J 1964 Smoothing and differentiation of data by simplified least squares procedures *Anal. Chem.* **36** 1627–39
Sellers P, Mintz Y, Sud Y E A and Dalcher A 1986 A simple biosphere model (SiB) for use within general circulation models *J. Atmos. Sci.* **43** 505–31
Sims D A, Rahman A F, Cordova V D, El-Masri B Z, Baldocchi D D, Bolstad P V, Flanagan L B, Goldstein A H, Hollinger D Y and Misson L 2008 A new model of gross primary productivity for North American ecosystems based solely on the enhanced vegetation index and land surface temperature from MODIS *Remote Sens. Environ.* **112** 1633–46
Sjöström M, Zhao M, Archibald S, Arneth A, Cappelaere B, Falk U, De Grandcourt A, Hanan N, Kergoat L and Kutsch W 2013 Evaluation of MODIS gross primary productivity for Africa using eddy covariance data *Remote Sens. Environ.* **131** 275–86
Stocker B D, Zscheischler J, Keenan T F, Prentice I C, Seneviratne S I and Peñuelas J 2019 Drought impacts on terrestrial primary production underestimated by satellite monitoring *Nat. Geosci.* **12** 264–70
Turner D, Ritts W, Styles J, Yang Z, Cohen W, Law B and Thornton P 2006 A diagnostic carbon flux model to monitor the effects of disturbance and interannual variation in climate on regional NEP *Tellus B: Chem. Phys. Meteorol.* **58** 476–90
Turner D P, Ritts W D, Cohen W B, Maeirsperger T K, Gower S T, Kirschbaum A A, Running S W, Zhao M, Wofsy S C and Dunn A L 2005 Site-level evaluation of satellite-based global terrestrial gross primary production and net primary production monitoring *Global Change Biol.* **11** 666–84
Turner D P, Ritts W D, Cohen W B, Gower S T, Running S W, Zhao M, Costa M H, Kirschbaum A A, Ham J M and Saleska S R 2006 Evaluation of MODIS NPP and GPP products across multiple biomes *Remote Sens. Environ.* **102** 282–92
Vermote E, Roger J C and Ray J P 2015 MODIS Surface Reflectance User's Guide: Collection 6, pp 1–40
Veroustraete F, Sabbe H and Eerens H 2002 Estimation of carbon mass fluxes over Europe using the C-Fix model and Euroflux data *Remote Sens. Environ.* **83** 376–99
Viovy N, Arino O and Belward A 1992 The best index slope extraction (BISE): a method for reducing noise in NDVI time-series *Int. J. Remote Sens.* **13** 1585–90
Wei S, Yi C, Fang W and Hendrey G 2017 A global study of GPP focusing on light-use efficiency in a random forest regression model *Ecosphere* **8** e01724
White M A, Thornton P E and Running S W 1997 A continental phenology model for monitoring vegetation responses to interannual climatic variability *Global Biogeochem. Cycles* **11** 217–34
Williams I, Torn M, Riley W and Wehner M 2014 Impacts of climate extremes on gross primary production under global warming *Environ. Res. Lett.* **9** 094011
Wolf S, Keenan T F, Fisher J B, Baldocchi D D, Desai A R, Richardson A D, Scott R L, Law B E, Litvak M E and Brunsell N A 2016 Warm spring reduced carbon cycle impact of the 2012 US summer drought *Proc. Natl Acad. Sci.* **113** 5880–5
Wu X, Xiao X, Zhang Y, He W, Wolf S, Chen J, He M, Gough C M, Qin Y and Zhou Y 2018 Spatiotemporal consistency of four gross primary production products and solar-induced chlorophyll fluorescence in response to climate extremes across CONUS in 2012 *J. Geophys. Res. Biogeosci.* **123** 3140–61
Xiao X, Zhang J, Yan H, Wu W and Biradar C 2009 Land surface phenology *Phenology of Ecosystem Processes* (Berlin: Springer) pp 247–70
Xiao X, Hollinger D, Aber J, Goltz M, Davidson E A, Zhang Q and Moore B III 2004a Satellite-based modeling of gross primary production in an evergreen needleleaf forest *Remote Sens. Environ.* **89** 519–34
Xiao X, Zhang Q, Braswell B, Urbanski S, Boles S, Wofsy S, Moore B III and Ojima D 2004b Modeling gross primary production of temperate deciduous broadleaf forest using satellite images and climate data *Remote Sens. Environ.* **91** 256–70
Yan H, Wang S.-q., Billesbach D, Oechel W, Bohrer G, Meyers T, Martin T A, Matamala R, Phillips R P and Rahman F 2015 Improved global simulations of gross primary product based on a new definition of water stress factor and a separate treatment of C3 and C4 plants *Ecol. Modell.* **297** 42–59
Yi C, Ricciuto D, Li R, Wolbeck J, Xu X, Nilsson M, Aires L, Albertson J D, Ammann C and Arain M A 2010 Climate control of terrestrial carbon exchange across biomes and continents *Environ. Res. Lett.* **5** 034007
Yuan W, Liu S, Zhou G, Zhou G, Tieszen L L, Baldocchi D, Bernhofer C, Gholz H, Goldstein A H and Goulden M L 2007 Deriving a light use efficiency model from eddy covariance flux data for predicting daily gross primary production across biomes *Agric. For. Meteorol.* **143** 189–207
Zhang F, Chen J M, Chen J, Gough C M, Martin T A and Dragoni D 2012 Evaluating spatial and temporal patterns of MODIS GPP over the conterminous US against flux measurements and a process model *Remote Sens. Environ.* **124** 717–29
Zhang L, Jiao W, Zhang H, Huang C and Tong Q 2017a Studying drought phenomena in the Continental United States in 2011

and 2012 using various drought indices *Remote Sens. Environ.* **190** 96–106

Zhang Y, Xiao X, Wu X, Zhou S, Zhang G, Qin Y and Dong J 2017b A global moderate resolution dataset of gross primary production of vegetation for 2000–2016 *Sci. Data* **4** 170165

Zhao M, Heinsch F A, Nemani R R and Running S W 2005 Improvements of the MODIS terrestrial gross and net primary production global data set *Remote Sens. Environ.* **95** 164–76

Zheng Y, Zhang L, Xiao J, Yuan W, Yan M, Li T and Zhang Z 2018 Sources of uncertainty in gross primary productivity simulated by light use efficiency models: model structure, parameters, input data, and spatial resolution *Agric. For. Meteorol.* **263** 242–57

Zhu H, Lin A, Wang L, Xia Y and Zou L 2016 Evaluation of MODIS gross primary production across multiple biomes in China using eddy covariance flux data *Remote Sens.* **8** 395

Zhu X, Pei Y, Zheng Z, Dong J, Zhang Y, Wang J, Chen L, Doughty R, Zhang G and Xiao X 2018 Underestimates of Grassland Gross Primary Production in MODIS Standard Products *Remote Sens.* **10** 1771